Biosensors and Bioelectronics 126 (2019) 565–571

Contents lists available at ScienceDirect

Biosensors and Bioelectronics

journal homepage: www.elsevier.com/locate/bios

An electric potential modulated cascade of catalyzed hairpin assembly and rolling chain amplification for microRNA detection

Shuang Wang[a,b], Shasha Lu[a,b], Jiahui Zhao[a,c], Jing Ye[b], Jianshe Huang[a,*], Xiurong Yang[a,b,c,**]

[a] State Key Laboratory of Electroanalytical Chemistry, Changchun Institute of Applied Chemistry, Changchun, Jilin 130022, China
[b] University of Science and Technology of China, Hefei, Anhui 230026, China
[c] University of Chinese Academy of Sciences, Beijing 100039, China

ARTICLE INFO

Keywords:
G-quadruplex
Catalyzed hairpin assembly
Rolling circle amplification
Cascade amplification
Electric potential
MiRNA

ABSTRACT

MicroRNAs serve as a new type of biomarker for multifarious diseases due to its critical roles in post transcriptional gene regulation. Herein, we firstly integrate the catalyzed hairpin assembly (CHA) and rolling circle amplification (RCA) into an electrochemical biosensor for sensitive and specific detection of miR-21. Meanwhile, an electric potential was employed to modulate the efficiency of CHA occurred on the electrode, which offer a simple but effective method to surmount the accessibility problem of probes. The biosensor achieved an ultrasensitive determination of miR-21 with a low limit of detection of 13.5 fM and a linear range from 15 fM to 250 pM. This research encourages us to challenge the hyphenated multiple amplification strategies and provides a stable and effective method for the detection of diseases-related miRNAs in peripheral biofluids, as well as paves a road for the future clinical diagnostics and treatment of disease.

1. Introduction

MicroRNAs (miRNAs) derived from precursor miRNA and matured by processing of endoribonucleases, then execute the function of mRNA cleave, mRNA degradation and translational inhibition by RNA-induced silencing complex assembly. (Chen et al., 2018) If above regulation mechanism is disturbed, aberrant mRNA translation will affect the expression level of protein and then induce the occurrence of some malignant diseases. (Pritchard et al., 2012) Furthermore, recently researchers found that miRNA was up or down regulated in peripheral biofluids, such as cerebrospinal fluid (CSF) and blood serum (SER) (Burgos et al., 2014), which enabled circulating cell-free miRNA as a potential and non-invasive biomarker candidate for monitoring multifarious diseases in early stage including cancer (Pritchard et al., 2012), cardiovascular diseases (Chen et al., 2017), kidney disease (Li et al., 2010) and neurodegenerative diseases (Cheng et al., 2013; Gao et al., 2010). Therefore, developing sensitive and reliable miRNA detection method is imperative and of great importance for analytical chemistry and biomedicine.

Due to intrinsic obstacles of miRNA including low abundance, small size, high sequence similarity among family members of miRNA and so on (Zhao et al., 2015), plentiful amplification methods have been used in a vast range of trace miRNA detection, such as strand displacement amplification (SDR) (Zhu et al., 2013), hybridization chain reaction (HCR) (Lu et al., 2017a), isothermal exponential amplification reaction, nuclease amplification (Gao et al., 2013; Yan et al., 2017), rolling circle amplification (RCA) (Wang et al., 2013; Xue et al., 2015, 2013), catalyzed hairpin assembly (CHA) (Dai et al., 2016) and nanomaterials based techniques (Liu et al., 2015; Liu et al., 2017). However, it is difficult to realize excellent performance of miRNA biosensor by single amplification, so more and more researchers devote themselves into hyphenating multiple amplifications methods. But the cascade of multiple amplification strategies is still in its infancy.

Among numerous traditional (microarrays, northern blotting and quantitative reverse transcription polymerase chain reaction (qRT-PCR)) and emerging methods (fluorescence (Lu et al., 2017b)), colorimetric, electrochemiluminescence (ECL), surface plasmon resonance (SPR) (Liu et al., 2017), and electrochemistry (Bai et al., 2017; Yao et al., 2017)), electrochemical method attracts considerable attentions due to rapid analysis, high sensitivity, minimal sample preparation and measurement time, no need for trained personnel, easily miniaturized and cost-effective apparatus. However, the electrochemical method is a typical solid-liquid surface technology, which could not circumvent probe accessibility problem inevitably. Therefore, researchers made their efforts to improve the accessibility of probes by Au−S bond (Levicky et al., 1998), biotin−NeutrAvidin interaction (Huang et al.,

* Corresponding author.
** Corresponding author at: State Key Laboratory of Electroanalytical Chemistry, Changchun Institute of Applied Chemistry, Changchun, Jilin 130022, China.
E-mail addresses: huangjs@ciac.ac.cn (J. Huang), xryang@ciac.ac.cn (X. Yang).

https://doi.org/10.1016/j.bios.2018.09.088
Received 25 July 2018; Received in revised form 20 September 2018; Accepted 27 September 2018
Available online 28 September 2018
0956-5663/

2014) and three-dimensional (3D) DNA tetrahedron nanostructure (Pei et al., 2010) to orderly immobilize probes, which actually had good performance comparing with that by random immobilization, and reached a better performance by controlling the concentration of probe. Besides above methods, extensive studies demonstrated electric bias potentials could work as a dynamic switch for the DNA conformation changing between a "lying" and a "standing" state and modulate the surface density of DNA that beneficial for the hybridization. (Arinaga et al., 2007; Edman et al., 1997; Kaiser and Rant, 2010; Rant et al., 2004a, 2004b) However, this effective theory has not been employed widely in the practical application as improving the detection performance of biosensor.

In the view of above advantages of electrochemical method, the effect of electric potential modulation and development tendency of miRNA determination, we proposed an electric potential modulated CHA-RCA cascade amplified electrochemical biosensor for miR-21 detection. The predominant amplified function was accomplished by combination of two amplification strategies of CHA and RCA, the synergetic amplified function is beneficial to the sensitivity of microRNA biosensor. Then the further improvement for the sensitivity was executed by the modulation of electric potential, which also effectively work out the accessibility problem of probes. The whole process is as follows briefly. We firstly modulated the density of hairpin probe1 (H1) by electric potential to guarantee efficient accomplishment of CHA at the first step. The improved CHA amplification enabled the target was employed circularly to obtain the template of second RCA amplification in abundance. Then RCA process amplified a host of repeated G4 that could capture the electroactive molecule, hemin, to give the final amplified electrochemical signal, which elevated the detection sensitivity effectively. In this paper, miR-21 was selected as target miRNAs because growing studies demonstrate that the aberrant expressions of miR-21 were associated with many powerful diseases such as cancer, neurodegenerative diseases and myocardial infarction (Chen et al., 2018). This strategy not only proves the possibility of integrating diversified amplification methods to sensitively detect low abundance miRNA, but also gives an evidence for the settlement of probe accessibility via electric potential modulation.

2. Experimental section

2.1. Materials and reagents

All DNAs and miRNAs were custom-synthesized by Sangon Biotechnology Co., Ltd. (Shanghai, China), and were dissolved in 10 mM Tris-HCl solution (pH 7.3, 200 mM NaCl) and water solution treated by diethyl pyrocarbonate (DEPC). The RNA solution could be used directly without any treatment. In order to make sure the DNAs formed the stable structure and hybridized effectively with other DNAs, the dissolved DNA solution were firstly heated at 95 ℃ for 5 min, then slowly cooled to room temperature with 6 ℃/min. The annealed sequences were accurately quantified by measuring the absorbance at 260 nm, then stored at 4 ℃ for further use. Potassium hexacyanoferrate (III) ($K_3Fe(CN)_6$), potassium ferrocyanide ($K_4Fe(CN)_6$), 6-Mercapto-l-hexanol (MCH), tris (2-carboxyethyl) phosphine hydrochloride (TCEP), and N-methyl mesoporphyrin IX (NMM) were purchased from Sigma-Aldrich (St Louis, MO). Phi 29 DNA polymerase, T4 DNA ligase, deoxyribonucleoside 5′-triphosphates mixtures (dNTPs) were obtained from Thermo Fisher Scientific. Methylene blue (MB) and hemin purchased from Sangon Biotechnology Co., Ltd. (Shanghai, China). MB were dissolved in 10 mM Tris-HCl solution (pH 7.3, 50 mM NaCl) for further use. Hemin solution (10 mM) was prepared by dissolving in DMSO, and then diluted to 0.5 mM by 10 mM Tris–HCl buffer solution containing 50 mM NaCl and 0.05% Triton X-100. All the solutions were prepared by the ultrapure water from Milli-Q water system with 18.25 MΩ. The detailed nucleic acid sequences used in experiments were shown in Table S1. The human blood serum was gratuitously provided by The Second Hospital of Jilin University.

2.2. Instrumentations

All of electrochemical tests were conducted on a CHI 660 A electrochemical workstation (Shanghai CH Instruments, China) with a conventional three electrode system composed of a functionalized gold electrode (Φ = 3 mm) as the working electrode, a platinum wire counter electrode, and an Ag/AgCl (3 M KCl) reference electrode. Fluorescence spectra were measured on an F-4600 FL spectrophotometer (Hitachi, Japan). UV–vis absorbance spectra were conducted at a CARY 500 UV–vis NIR Varian spectrophotometer. Nucleic acid electrophoresis apparatus (Tanon, EPS 300) was employed to implement native polyacrylamide gel electrophoresis (PAGE).

2.3. Electrode treatment and functionalization of sensing surface

The electrode cleaning process was consistent with previous report (Wei et al., 2015). Briefly, the soaked gold electrode with piranha solution was successively polished with 1 μm, 0.3 μm, and 0.05 μm alumina slurry and underwent thorough rinse with ultrasonic treatment in ethanol and double-distilled water. Then, the electrode was immersed in 50% nitric acid for 30 min to further clean the electrode surface. Finally, 0.5 M H_2SO_4 was used to the electrochemical clean of electrode until a typical and stable characteristic peak appeared. Next we executed the functionalization of sensing surface. 2 μM hairpin probe 1 (H1) with thiol was incubated with 1 mM TCEP for 30 min at room temperature to break the disulfide bond. The dried electrode with nitrogen gas was modified with TCEP-pretreated H1 (10 μL) overnight at 4 ℃ to obtain Au/H1. Then − 0.4 V was applied for 5 s to Au/H1 in 10 mM PBS buffer (pH 7.4, 100 mM NaCl) containing 1 mM MCH to control the density of H1 on the electrode surface. After that, 10 μL of MCH (1 mM) in 10 mM Tris-HCl solution (50 mM NaCl, pH 7.3) was dropped on the electrode and incubated for 1 h at 4 ℃ to fully block the uncombined sites. This functionalized layer was named as Au/H1/MCH. Subsequently 10 μL solution containing different concentration miRNAs (T) and 2 μM hairpin probe 2 (H2) were dropped on the electrode surface to execute the CHA process at room temperature for 2 h, obtaining layer Au/H1/MCH/T-H2. It is note that rinsing thoroughly with washing solution (10 mM Tris-HCl, pH 7.3, 50 mM NaCl and 0.05% Tween-20) after each modification is necessary.

2.4. Process of electric potential modulation

A potentiostat was utilized to control the voltage applied on the Au working electrodes. First, the typical amperometric i-t curve was operated on the 2 μM H1-saturated electrode in 10 mM PBS buffer (pH 7.4, 100 mM NaCl) containing 1 mM MCH. The voltage was set ranging from 0 V to − 0.6 V, and the run time was set 5 s, which was enough to change the density of H1 (Kaiser and Rant, 2010). MB molecules, can specifically intercalate into DNA duplex, were used as electrochemical probe. Au/H1/MCH obtained at different modulation potential and the corresponding Au/H1/MCH/T-H2 obtained by reacting with 1 μM T and 2 μM H2 incubated with 10 μL MB (1 mM) for 30 min in dark at room temperature to obtain Au/H1/MCH/MB and Au/H1/MCH/T-H2/MB. After rinsing with 10 mM Tris-HCl (pH 7.3, 50 mM NaCl and 0.05% Tween-20), differential pulse voltammetry (DPV) response of Au/H1/MCH/MB and Au/H1/MCH/T-H2/MB were measured in MB-free 10 mM Tris − HCl (pH 7.3, 50 mM NaCl). The potential ranged from 0.1 V to − 0.6 V. The peak current differences between Au/H1/MCH/MB and Au/H1/MCH/T-H2/MB were used to evaluate the efficiency of CHA that acted as a standard for choosing optimum electric potential.

2.5. Production of electrochemical signal based on RCA accomplishment with generation plenty of hemin/G-quadruplex complexes

The successful achievement of CHA process provides a template for RCA process, and the RCA process was accomplished according to the following procedure. Briefly, 10 μL of a solution containing 10 × ligase buffer, 0.2 U T4 DNA ligases and 1 μM C-DNA were dropped on the layer Au/H1/MCH/T-H2 at 25 ℃ for 1 h. The linked c-DNA by itself will execute the RCA process under the assistance of 1 mM dNTPs and 0.5 U phi 29 DNA polymerase at 37 ℃ for 1 h. The electrode modified with plentiful G4 was incubated with 10 μL hemin solution (0.5 mM) for 2 h in dark at room temperature to form hemin/G4 complexes. After rinsing with 10 mM Tris-HCl (pH 7.3, 50 mM NaCl and 0.05% Tween-20), DPV measurement was carried out in Tris − HCl solution (10 mM, pH 7.3) containing 50 mM NaCl, and the experiment parameters were as follows: initial potential: − 0.1 V, final potential: − 0.6 V, pulse amplitude: 0.01 V, pulse width: 0.05 s, sampling width: 0.0167 s. The electrochemical signal was related to the concentration of target miRNA.

2.6. MiR-21 detection in human serum

Human blood serum sample was diluted with 10 mM Tris − HCl (pH 7.3, 50 mM NaCl) to the concentration of 2%. A certain amount of miR-21 s with known concentrations were added to the diluted human blood serum as mimic real sample and then mixed with 2 μM H2 to achieve the subsequent CHA and RCA process on the electrode. All other experimental processes are same as those described in Sections 2.3–2.5. Finally, the detected concentrations by the biosensor and the spiked concentrations were compared.

3. Results and discussion

3.1. Design principle of electric potential modulated CHA-RCA amplification for miRNA detection

As displayed in Scheme 1, H1 with thiol on the 3′ termini was immobilized on the Au electrode by Au-S binding. After H1 saturated on the electrode, the negative electric potential was applied to control the density and conformation of H1. The 5′ termini of H1 could capture target miRNA (T), but was partially closed in the stem of H1. The hybridization with T released the 3′ termini of H1 that could open and bind with H2 via toehold displacement reaction. While a few H2 bind with H1 in absence of assistance from T even though containing most of the complementary sequences of H1. Once the reaction of H1 and H2 was triggered, the T will be competed with H2 and finally replaced into solution. The released T was employed circularly to initiate the next circle. Above process adequately executed the CHA function. As the finishing of CHA process, plenty of H1-H2 duplexes with tail were obtained. The tail could bind with c-DNA and form a circle template under the aid of T4 DNA ligase. Meanwhile, the phi 29 DNA polymerase and dNTPs worked as raw materials for RCA on tail. The achievement of RCA process would produce abundant guanines those form G4 under the stabilization of cation. Then significantly amplified current response was obtained after capturing electrochemical probe hemin. The electrochemical signal was linearly dependent on the amounts of target miRNA. On the basis of above design, we implemented electric potential modulated CHA-RCA amplification for miR-21 detection.

3.2. Polyacrylamide gel electrophoresis (PAGE), fluorescence spectral and electrochemical characterization of surface functionalization

In order to make sure the feasibility of design principle, we resort to PAGE and fluorescence spectra to verify the CHA-RCA combination. (The relevant experiment details were displayed in supporting information.) As shown in Fig. 1A, when no target miRNA existed, lane 6

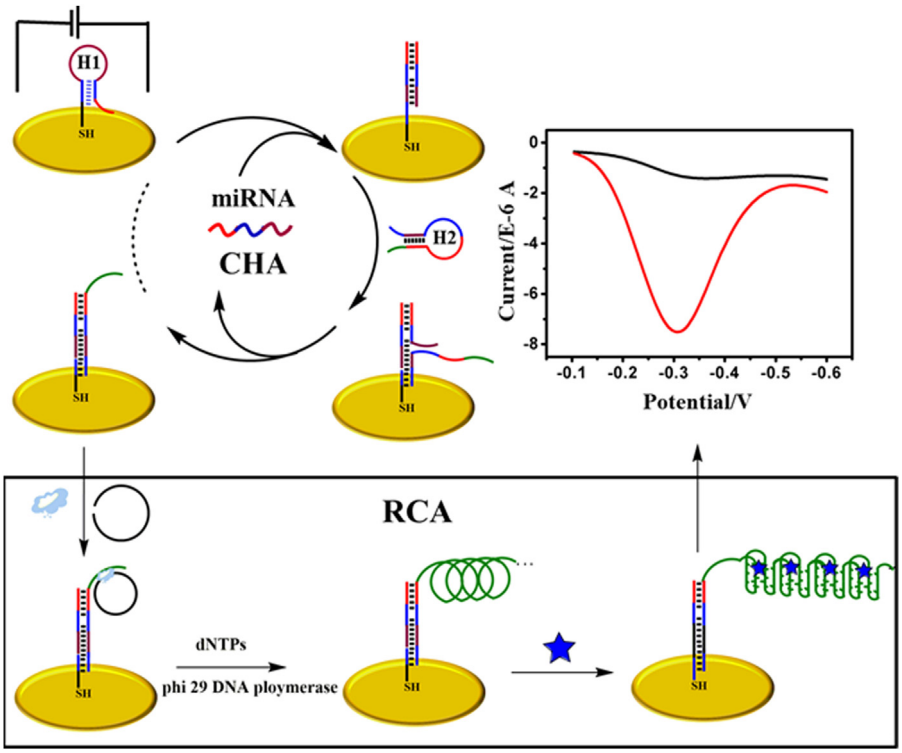

Scheme 1. Schematic illustration of potential modulation for detection of microRNA based on cascade of catalyzed hairpin assembly (CHA) and rolling chain amplification (RCA).

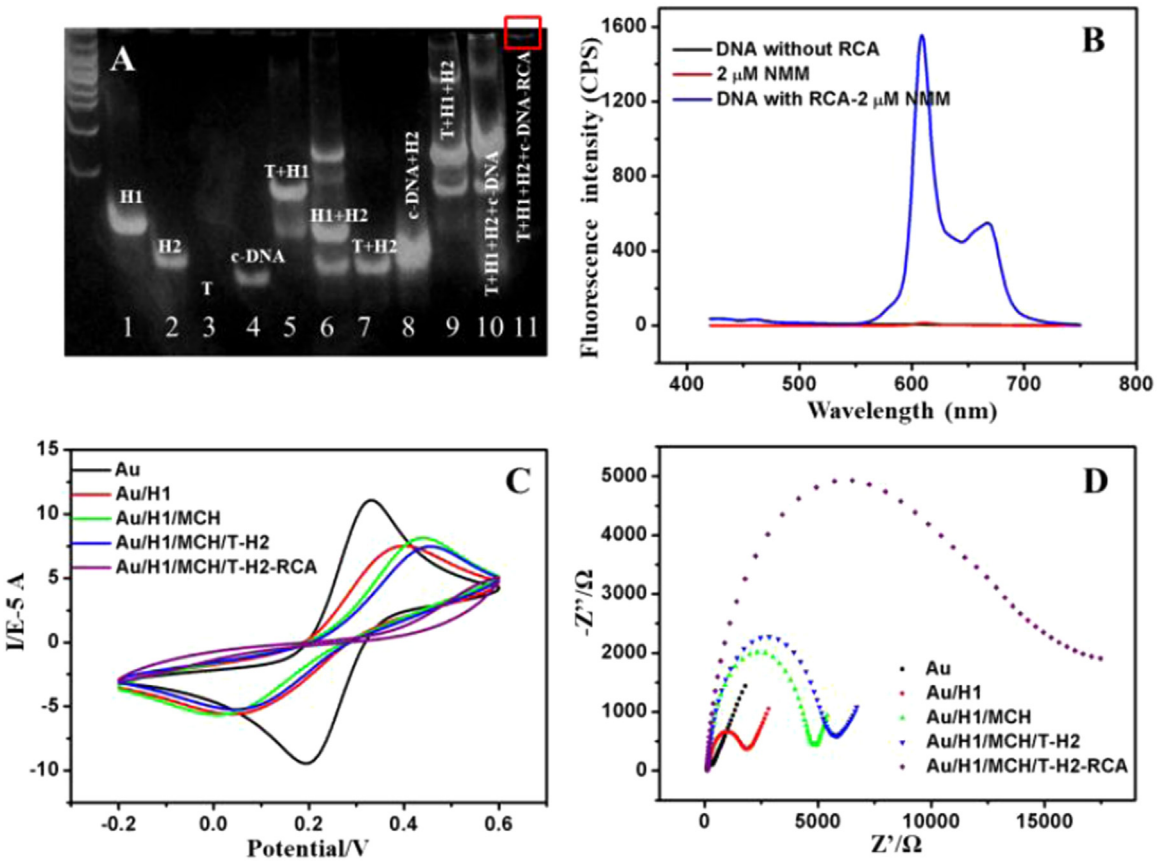

Fig. 1. PAGE (A) and fluorescence spectra (B) of CHA-RCA products; CV (C) and EIS (D) measurement for different functionalized electrodes in 0.1 M KCl solution containing 5.0 mM $[Fe(CN)_6]^{3-/4-}$. The potential range: − 0.2 − 0.6 V, the scan rate: 100 mV s^{-1}; the frequency range: 0.1 − 10^5 Hz.

showed the H1 and H2 bands with a weak band for the hybridization product. While under the help of T, the band of hybridization product turned stronger (lane 9), which meant that T contributed to the production of H1-H2 duplex. Lane 10 shifted slower than lane 9 because c-DNA bound with H1-H2 duplex. The highest and only one band in lane 11 ascribed to the slow motion speed of longer sequences, demonstrating the successful combination of CHA-RCA. While the control experiments in lane 1, 2, 3, 4, 5, 7, 8 showed the hybridization conditions of other DNA combinations, further proved that T played a critical role in accomplishment of CHA-RCA. NMM, an anionic porphyrin, demonstrates excellent structural selectivity for G4 over single/double strand and triplex. NMM emits faint fluorescence by itself, while it strongly binds with G4 accompanying by enhanced fluorescence (Oh et al., 2010). The fluorescence spectra (Fig. 1B) also exhibited that only the CHA-RCA amplified sequences (blue line) show the strongest fluorescence comparing with the only NMM dye (red line) and DNA without RCA (black line), which indicated above designed probes could execute the function of producing plenty of repeated G4. Under above feasible premise, we built sensor layers step by step on the electrode. As shown in Fig. 1C, the well-defined CV redox peaks at bare Au electrode was significantly decreased when H1 was immobilized on the surface because H1 inhibited the transfer of electron. After blocking with MCH, the CV signal continued to decline due to its nonelectroactive property. When H2 hybridized with H1 under the assistance of T, the redox peaks further decreased, which ascribe to the hindrance of longer duplex for electron transfer. Until the RCA accomplished, the CV response reduced to minimum due to generation of a host of G-rich sequences. The corresponding impedance spectra in Fig. 1D showed that the electron-transfer resistance constantly increased as H1, MCH, T-H2 were modified on the electrode in sequence, and increased dramatically when RCA accomplished on the sensing surface. These electrochemical characterizations verify that the miR-21 sensing surface was successfully constructed just as what we designed.

3.3. Optimization of electric potential applied on electrode

The density and conformation of capture probes plays a critical role in the hybridization efficiency, which had been confirmed by previous reports (Huang et al., 2014; Wang et al., 2017). The intrinsically negatively charged DNA could stand upright or lie on the electrode surface when negative or positive bias was applied. (Rant et al., 2004) Therefore, we control the density and conformation of probes from fountainhead by modulating H1. Before applying voltage to modulate the density, we should clear and definite the saturability of H1. As displayed in Fig. 2A and B, the impedance increased and the typical redox peaks declined until the concentration increased to 2 μM, then were nearly unchanged even though the concentration increased continuously, which was consistent with previous reference (Huang et al., 2013). After incubating electrode with saturated H1, we control the density of H1 by externally applied negative bias. Fig. 2C exhibits that the impedance constantly decreased as more and more negative voltage was exerted on electrode, which verified that negative potential effectively repel the DNAs from the surface and lead to the constantly shedding of partial H1 (Kaiser and Rant, 2010). Furthermore, researchers reported that electric field could direct nucleic acid hybridization (Edman et al., 1997). Thus we optimized the applied electric potential by evaluating the hybridization efficiency. MB was used as electrochemical probe due to its property that specifically intercalating into DNA duplex (Kelley et al., 1997; Wu et al., 2015). Therefore, we investigated the hybridization efficiency by comparing the combined quantity of MB on the duplex. The process of CHA and capturing MB is schematically demonstrated in Fig. S1. As different negative bias was

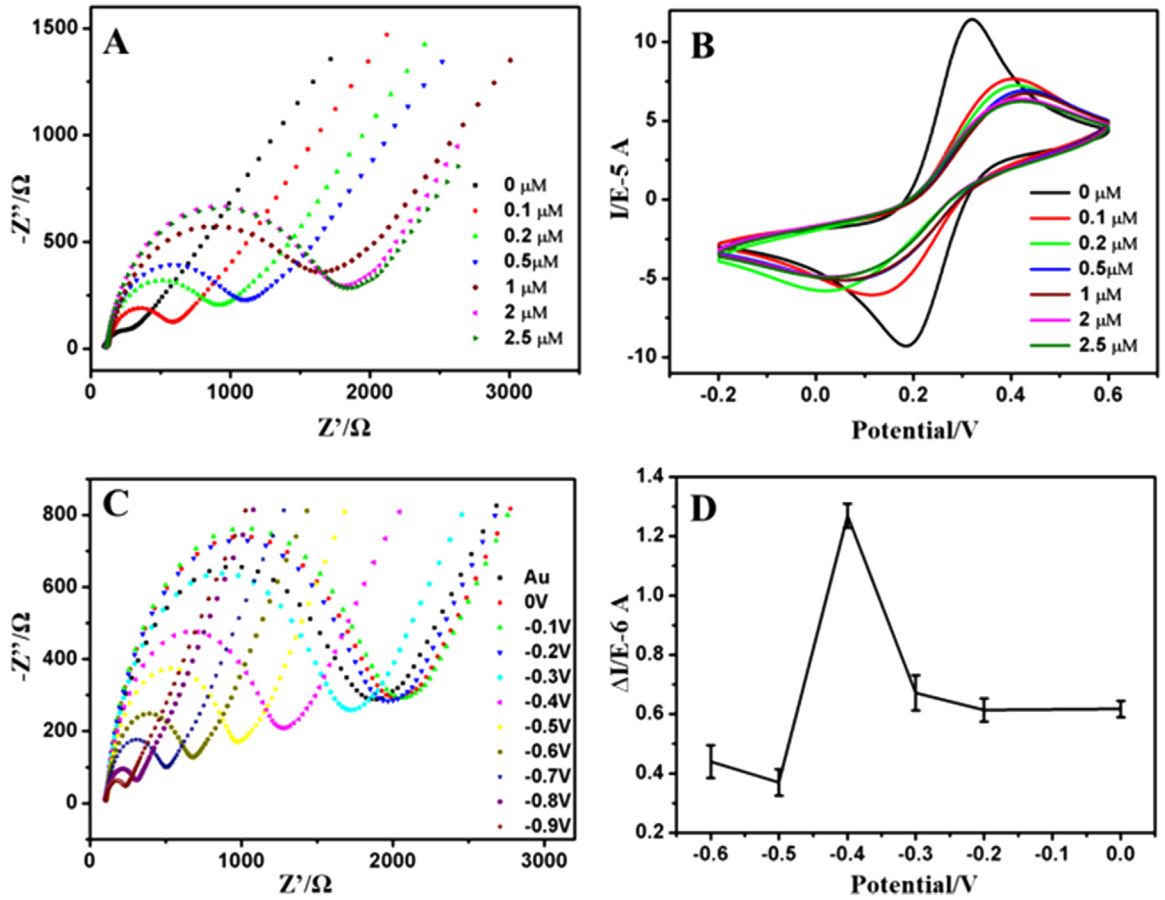

Fig. 2. Optimization of H1 concentration and applied electric potentials. EIS (A) and CV (B) measurements of H1 with different concentration modified electrode. The concentrations range from 0 to 2.5 μM. EIS changes (C) of 2 μM H1 modified surface after applying different electric potential. The electric potentials range from 0 to − 0.9 V. Current difference (D) between Au/H1/MCH/MB and Au/H1/MCH/T + H2/MB after applying different electric potentials on the 2 μM H1 modified electrode surface. The error bars were obtained by three parallel measurements.

applied on the electrode, H1 with different density and conformation stood on the surface. Due to the intrinsic hairpin structure of H1, the short hybridized sequence could accommodate MB and produce DPV signal (I_1, Fig. S1A'). When the CHA process accomplished after introducing T and H2, the obtained longer duplexes captured more MB, producing stronger current signal (I_2, Fig. 1B and B′). The hybridization efficiency could be reflected by variation of peak current ($\Delta I = I_2 - I_1$) that act as a standard for choosing optimum electric potential. Fig. 2D shows that ΔI is largest when the potential is − 0.4 V. Therefore, we chose − 0.4 V as the optimum electric potential. For the reason, we conjectured that the more negative voltage would lead to large amounts of shedding of H1, and the limited duplexes have lower current response; while the more positive potential made the density and conformation of H1 unfavorable to achieve CHA process because the mutual steric hindrance of serried H1 suppressed the hybridization, also showing lower current signal. These results were consistent with previous report (Arinaga et al., 2007).

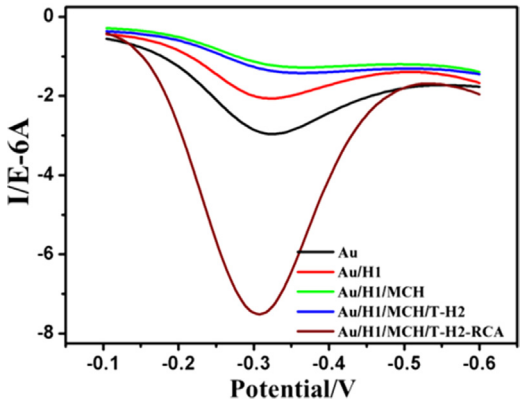

Fig. 3. Electrochemical performance of proposed biosensor. DPV measurement of different modified layers including Au, Au/H1, Au/H1/MCH, and Au/H1/MCH/T-H2, and Au/H1/MCH/T-H2/RCA after incubating with 0.5 mM hemin.

3.4. Electrochemical performance of proposed miR-21 biosensor

The electrochemical signal recorded by DPV was obtained from the redox property of hemin. When hemin was locked into the G4, it would approach the electrode surface, exhibiting increased current signal. On the basis of above signal generation mechanism, we assess the ability of modified layers to capture hemin by DPV measurements via optimum electric potential modulation because the numbers of G4 are proportional to the amounts of hemin and the final electrochemical signal comes from above captured hemin. As shown in Fig. 3, there is a small current response in layers Au, Au/H1, Au/H1/MCH, and Au/H1/MCH/T-H2, which might attribute to the nonspecific adsorption (Shi et al., 2017). Furthermore, as the addition of probes, the current deceased partially, representing the nonspecific adsorption of hemin was inhibited when probes modified on the electrode in succession. When Au/H1/MCH/T-H2/RCA layer formed on the sensor surface, the peak current was significantly enhanced, which caused by a load of G4 produced on the electrode and a great deal of hemin captured by G4. These results suggested that our proposed miR-21 biosensor had good

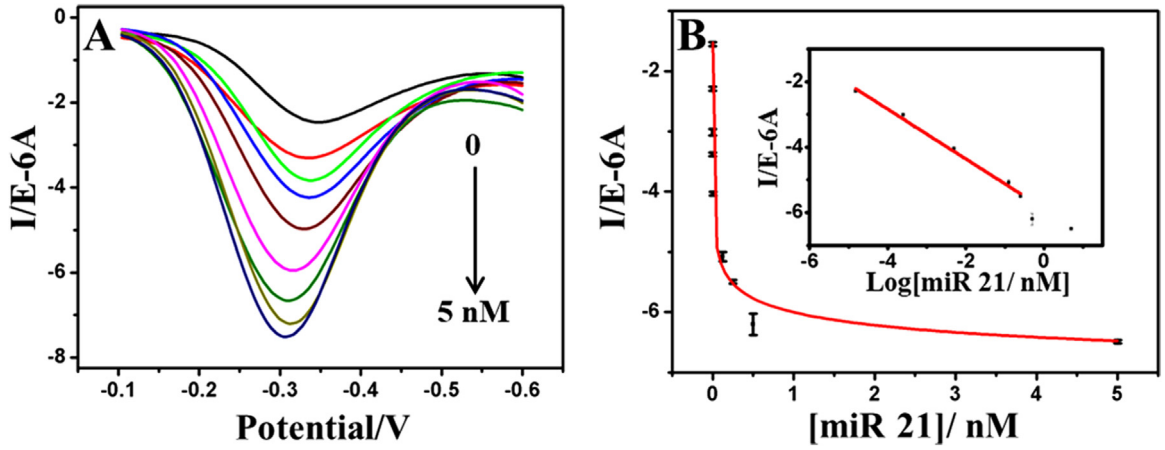

Fig. 4. Linearity of our designed biosensor. DPV measurement (A) of the proposed electric potential-modulated CHA-RCA biosensor for miRNA with increasing concentration ranging 0–5 nM (0, 15 fM, 250 fM, 500fM, 5 pM, 125 pM, 250 pM, 500 pM, 5 nM). (B) Plot the current intensity of the logarithm of miR-21 concentration. The error bars represent the standard deviation of three measurements.

electrochemical performance and proved the feasibility of the designed system again. Furthermore, we also constructed the biosensor with the same procedure but without the electric potential modulation step. Under the same experimental conditions, DPV response of the biosensor with electric potential modulation is 1.6 times stronger than that without electric potential modulation (Fig. S2), which suggested the electric potential modulation could efficiently improve the performance of biosensor.

3.5. Detection of miR-21

On the basis of design principle and optimization for applied potential, we carried out quantitative analysis for miR-21 by DPV. As demonstrated in Fig. 4A, the current response enhanced as the increase of miR-21 concentration, which was in accord with what we designed. Furthermore, the DPV response was linearly dependent on the logarithm of mi-21 concentration from 15 fM to 250 pM The limit of detection was as low as 13.5 fM for miR-21 based on 3 S/N. We compared our proposed strategy with other miRNA biosensors in Table S2, the results displayed that the LOD of our method was comparable to some strategies. Meanwhile, comparing with other signal amplified strategies, our method was the first try for the cascade amplification of CHA and RCA via hybridization reaction. Additionally, such dual-amplified function was further boosted by applying constant voltage to modulate the density and conformation of probes without fussy and expensive preparation of nanomaterials. Taking 1 pM and 20 pM concentrations as example, we investigate the reproducibility of our method. Both of their RSDs were less than 3%. As we mentioned earlier, the advantages of our designed biosensor portended that combination of diversified amplification strategies actually provide innovative solutions with potential for trace determination.

3.6. Sensitivity and specificity of miR-21 biosensor

In order to evaluate the specificity of the fabricated biosensor, we investigated the DPV response of different miRNAs including miR-21, miR-128, miR-134, hsa-miR-30e-5p, hsa-miR-18b-5p, and hsa-miR-342-5p under the same experiment condition only substituting the targets. The results in Fig. 5 represented that only the target miR-21 had a large DPV response and other control samples had small current response, demonstrating that only the target could trigger the cascade of CHA and RCA and gave amplified electrochemical signal. All of above results suggested the excellent selectivity of this biosensor for target miRNA detection. Therefore, such miR-21 electrochemical biosensor with excellent sensitivity and specificity has potential for practical analysis.

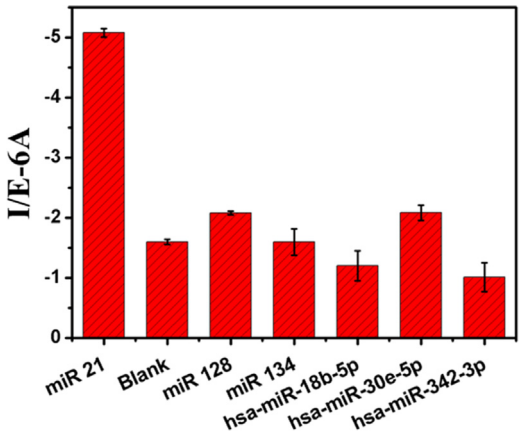

Fig. 5. Selectivity of the proposed biosensor. Comparing the current response of target miR-21 with control samples including blank, miR-128, miR-134, hsa-miR-30e-5p, hsa-miR-18b-5p, and hsa-miR-342–5p. The concentration of all samples was 125 pM The error bars were obtained based on three measurements.

3.7. Electrochemical analysis of miR-21 in human serum

To investigate the practical utility of our biosensor, we evaluated its analytical function in biological matrix. Employing such electric potential modulated CHA-RCA cascade method, we keep the DNA frame and raw materials that achieving CHA and RCA constant just replacing the Tris-HCl buffer solution with 2% human blood serum, meanwhile quantified the spiked miRNA with different concentrations by measuring the DPV response. The statistics in Table S3 indicated that the measured quantities were close to the spiked amounts, and has a satisfactory recovery from 92.8% to 101.1% and RSD ranging 0.004% − 3.23%. These results prove the potential-modulated CHA-RCA electrochemical biosensor has the promise to develop to be portable devices for medical detection in peripheral fluids.

4. Conclusions

In summary, we fabricate an electric potential modulated CHA-RCA electrochemical platform for sensitive and selective determination of miR-21. First, the combination of CHA and RCA is utilized to amplify abundant G4 sequences, which captures hemin to produce amplified

electrochemical signal. Second, we make use of simple and facile approach that modulation of electric bias potentials to control the conformation and density of probe, which is beneficial for the hybridization efficiency of CHA. By integrating dual cascade amplification and potential modulation, such miR-21 biosensor exhibits excellent performance in sensitivity with a low detection limit of 13.5 fM. The biosensor also shows good selectivity, and can be applied to reliably determine miR-21 in human blood serum. Our proposed method not only has potential to apply in diagnosis and treatment of miRNA-associated diseases, but also to detect other targets that specifically bind with functional DNAs or aptamer in the future.

Acknowledgment

This work was financially supported by the National Natural Science Foundation of China (No. 21627808, 21435005), Key Research Program of Frontier Sciences, CAS (QYZDY-SSW-SLH019), and the Development Project of Science and Technology of Jilin Province (No. 20170101195JC).

Declarations of interest

None.

Appendix A. Supplementary material

Supplementary data associated with this article can be found in the online version at doi:10.1016/j.bios.2018.09.088.

References

Arinaga, K., Rant, U., Knežević, J., Pringsheim, E., Tornow, M., Fujita, S., Abstreiter, G., Yokoyama, N., 2007. Biosens. Bioelectron. 23, 326–331.
Bai, H.P., Wang, C.Q., Cao, Q.E., 2017. Chin. J. Anal. Chem. 45, 1535–1541.
Burgos, K., Malenica, I., Metpally, R., Courtright, A., Rakela, B., Beach, T., Shill, H., Adler, C., Sabbagh, M., Villa, S., Tembe, W., Craig, D., Van Keuren-Jensen, K., 2014. PLoS One 9, e94839.
Chen, Y.X., Huang, K.J., Niu, K.X., 2018. Biosens. Bioelectron. 99, 612–624.
Chen, Z., Li, Y., Dian, K., Rao, L., 2017. Theranostics 7, 2287–2288.
Cheng, L., Quek, C., Sun, X., Bellingham, S., Hill, A., 2013. Front. Genet. 4, 1–11.
Dai, J., He, H., Duan, Z., Zhou, C., Long, Y., Zheng, B., Du, J., Guo, Y., Xiao, D., 2016. J. Mater. Chem. B 4, 3191–3194.
Edman, C.F., Raymond, D.E., Wu, D.J., Tu, E., Sosnowski, R.G., Butler, W.F., Nerenberg, M., Heller, M.J., 1997. Nucleic Acids Res. 25, 4907–4914.
Gao, F., Lei, J., Ju, H., 2013. Chem. Commun. 49 (68), 7561–7563.
Gao, J., Wang, W.Y., Mao, Y.W., Gräff, J., Guan, J.-S., Pan, L., Mak, G., Kim, D., Su, S.C., Tsai, L.-H., 2010. Nature 466, 1105.
Huang, F., Xu, P., Liang, H., 2014. Biosens. Bioelectron. 51, 317–323.
Huang, L., Wu, J.J., Zheng, L., Qian, H.S., Xue, F., Wu, Y.C., Pan, D.D., Adeloju, S.B., Chen, W., 2013. Anal. Chem. 85, 10842–10849.
Kaiser, W., Rant, U., 2010. J. Am. Chem. Soc. 132, 7935–7945.
Kelley, S.O., Barton, J.K., Jackson, N.M., Hill, M.G., 1997. Bioconj. Chem. 8, 31–37.
Levicky, R., Herne, T.M., Tarlov, M.J., Satija, S.K., 1998. J. Am. Chem. Soc. 120, 9787–9792.
Li, J.Y., Y, Y.T., Z, M.M., M, G.J., 2010. Nephrology 15, 599–608.
Liu, R.J., Wang, Q., Li, Q., Yang, X.H., Wang, K.M., Nie, W.Y., 2017. Biosens. Bioelectron. 87, 433–438.
Lu, S., Hu, T., Wang, S., Sun, J., Yang, X., 2017a. ACS Appl. Mater. Interfaces 9, 167–175.
Lu, S., Wang, S., Zhao, J., Sun, J., Yang, X., 2017b. Anal. Chem. 89, 8429–8436.
Oh, S.S., Plakos, K., Lou, X.H., Xiao, Y., Soh, H.T., 2010. Proc. Natl. Acad. Sci. USA 107, 14053–14058.
Pei, H., Lu, N., Wen, Y., Song, S., Liu, Y., Yan, H., Fan, C., 2010. Adv. Mater. 22, 4754–4758.
Pritchard, C.C., Cheng, H.H., Tewari, M., 2012. Nat. Rev. Genet. 13, 358.
Rant, U., Arinaga, K., Fujita, S., Yokoyama, N., Abstreiter, G., Tornow, M., 2004a. Nano Lett. 4, 2441–2445.
Rant, U., Arinaga, K., Fujita, S., Yokoyama, N., Abstreiter, G., Tornow, M., 2004b. Langmuir 20, 10086–10092.
Shi, K., Dou, B.T., Yang, J.M., Yuan, R., Xiang, Y., 2017. Biosens. Bioelectron. 87, 495–500.
Wang, S., Lu, S., Zhao, J., Huang, J., Yang, X., 2017. ACS Appl. Mater. Interfaces 9, 41568–41576.
Wang, X.P., Yin, B.C., Wang, P., Ye, B.C., 2013. Biosens. Bioelectron. 42, 131–135.
Wei, T., Dong, T., Wang, Z., Bao, J., Tu, W., Dai, Z., 2015. J. Am. Chem. Soc. 137, 8880–8883.
Wu, X., Chai, Y., Zhang, P., Yuan, R., 2015. ACS Appl. Mater. Interfaces 7, 713–720.
Xue, Q., Lv, Y., Xu, S., Zhang, Y., Wang, L., Li, R., Yue, Q., Li, H., Gu, X., Zhang, S., Liu, J., 2015. Biosens. Bioelectron. 66, 547–553.
Xue, Q., Wang, L., Jiang, W., 2013. Chem. Commun. 49, 2640–2642.
Yan, Y., Yue, S., Zhao, T., Luo, B., Bi, S., 2017. Chem. Commun. 53, 12201–12204.
Yao, X.L., Chen, Z.D., Zhang, J., Cui, H.F., Lin, Y., Hong, N., He, L.L., Kong, D.R., Fan, H., Cheng, L., 2017. Chin. J. Anal. Chem. 45, 1421–1426.
Zhao, Y., Chen, F., Li, Q., Wang, L., Fan, C., 2015. Chem. Rev. 115, 12491–12545.
Zhu, J., Zhang, L., Dong, S., Wang, E., 2013. ACS Nano 7, 10211–10217.